Self-healing assessment of cementitious mortars through ultrasonic monitoring

Lefever, Gerlinde; Van Hemelrijck, Danny; Snoeck, Didier; Angelis, Dimitrios

Published in:
Cement and Concrete Composites

DOI:
10.1016/j.cemconcomp.2022.104683

Publication date:
2022

Self-healing assessment of cementitious mortars through ultrasonic monitoring.

Gerlinde Lefever[a*], Danny Van Hemelrijck[a], Didier Snoeck[a,b], Dimitrios G. Aggelis[a]

[a] Department Mechanics of Materials and Constructions, Vrije Universiteit Brussel (VUB), Pleinlaan 2, 1050 Brussels, Belgium

[b] BATir Department, Université Libre de Bruxelles (ULB), 50 F.D. Roosevelt Avenue, 1050 Brussels, Belgium

* Correspondence: Gerlinde.Lefever@vub.be; Tel. +32 (0)2 629 29 27

Abstract: Self-healing cementitious composites have gained increased attention over the past decades, encouraged by the excessive costs related to manual concrete repair. Thorough investigations on these materials have shown their potential to be applied for real life construction elements. However, the existing methods used to assess the self-healing effectiveness possess several limitations, making an in-situ evaluation of the regained properties practically impossible. This study therefore investigates a non-destructive testing methodology based on ultrasonic wave propagation that can eventually be practically implemented. The sensitivity of ultrasound to the elastic properties of the material under study allows to assess the self-healing effectiveness and discriminate between actual healing, in the sense of mechanical properties restoration, and simple filling of the crack. Moreover, the method is validated and complemented by numerical wave simulations that allow to connect the macroscopically measured wave velocity to the stiffness of the healing products deposited within the crack.

Keywords: Cement; Self-Healing; Ultrasound; Wave simulations; Superabsorbent Polymer (SAP); hydrogel; Nanosilica.

1. Introduction

Since its first use in the mid-1800s, Portland-based concrete has become the most-used construction material. Due to its extensive usage, the maintenance and repair of concrete structures became equally important. However, manual repairs are costly, labour-intensive and limited by the accessibility of the structural element. For this reason, self-healing cementitious materials have attracted the attention of researchers around the world, which eliminate the previously mentioned issues and allow repairs to take place in a timely, automated manner. This process, called autogenous healing, allows to recover the water tightness (self-sealing) and to restore the mechanical performance (self-healing) of cracked elements. Autogenous healing consists of two main mechanisms, being the further hydration of unhydrated cement particles and the precipitation of $CaCO_3$ by the dissolution and carbonation of $Ca(OH)_2$ present inside the crack [1] [2]. These processes occur simultaneously, though the continued hydration mostly takes place at early age, when unhydrated cement is still available, while the precipitation of $CaCO_3$ becomes more prominent at later age [3]. It should be mentioned that for these chemical processes to occur, water is essential to be present inside the cracks. As a result, the promotion of autogenous healing can be accomplished by maintaining the humidity within the cracks, which is most commonly done by the addition of superabsorbent polymers (SAPs) [4] [5] [6]. As their name implies, SAPs are able to absorb large amounts of water. When present inside the crack,

the SAPs absorb water from the outer environment, thereby physically blocking the crack entrance, and retain this moisture until the relative humidity decreases. The absorbed water is then released inside the crack and drives the hydration of cement and the calcite precipitation. In addition to the above mentioned two healing processes, a third autogenous healing mechanism includes the pozzolanic reaction of CH into CSH within aqueous media. In this case, a pozzolanic source should be present within the matrix, which can be achieved by the addition of nanosilica. These nanoparticles are mostly used to obtain improved mechanical properties and durability of cementitious materials [7] [8] [9]. As nanosilica is a highly-reactive, pozzolanic material, it is capable to rapidly transform CH to CSH in aqueous media, which contributes to the promotion of self-healing [10]. Moreover, previous investigations on the combination of nanosilica and superabsorbent polymers in cementitious composites show their compatibility [11] [12], meaning that the mixtures benefit from the inclusion of both additives as the macro pore formation by the SAPs and corresponding possible decrease in mechanical properties can be enhanced by the increase in strength caused by the nanosilica addition.

The use of SAPs and/or nanosilica within cementitious mixtures has clearly shown its potential for self-healing purposes [3] [4] [6] [10] [13]. To evaluate the self-healing effectiveness, various testing techniques are available, depending on the feature to be investigated. The visual crack closure can be studied by means of microscopic analysis [14], but only provides information on the filling at the surface. Filling within the crack depth can be studied by X-ray tomography [4] [15], but then again it does not provide any guarantee on a physical connection between the crack walls. To assess the water tightness or self-sealing ability, water permeability tests are often used [16] [17]. Still, to determine the regained mechanical performance, mechanical tests are necessary [18]. The use of these intrusive or destructive evaluation methods would be impossible for operational structures, while a confirmation of the regained mechanical properties is necessary to ensure a structure's safety. These issues lead to the development of a non-destructive testing protocol that allows for an estimation of the load-bearing capacity after healing.

A technique that has demonstrated promising results is ultrasonic wave monitoring. Ultrasound is sensitive to the microstructural developments and the elastic properties of the material it travels through. In case of cementitious materials, ultrasound has mainly been adopted to monitor the hardening process [19] [20], estimate the mechanical properties [21] [22] [23], identify damage [24] [25] [26] and, more recently, also to monitor the repair and healing process [27] [28] [29] [30] [31]. The latter study comprised the monitoring of the self-healing effectiveness through surface wave measurements, which were able to distinguish between the uncracked, cracked and healed state, as the wave velocity and amplitude decreased upon cracking and restored when healing products were formed inside the crack. Still, a limitation of the method is that the studied wave parameters depend on the entire propagation path, which includes both the cracked/healed zone and the intact mortar around. While the outcome provides interesting information on the restoration during healing, the effect of the healed layer was not separated from these results and thus the stiffness of the healing products was not determined. An evaluation of these elastic properties will be crucial to assess the self-healing ability, since a stiff connection between the crack walls is essential to obtain mechanical restoration. A means to achieve this objective is the use of numerical wave simulations that offer the capacity to alter the elastic properties of the crack model under study and thus to examine the correspondence between the macroscopically measured wave velocity and the stiffness of the healing material, without being masked by the rest of the uncracked material between the sensors. Additionally, the effect of only partially filled cracks can be studied, which is a valid assumption based on literature studies [32].

In this study, cementitious mixtures with and without SAPs and/or nanosilica were investigated. Apart from the expected self-healing, the most important objective in this study is the estimation of the healing product's stiffness through ultrasonic assessment. Elastic wave parameters, like ultrasonic wave velocity and attenuation, are measured to qualitatively reveal restoration of the propagation path. The experimental trends are then combined with

numerical results in order to lead to the actual stiffness of the healing products for the first time, quantifying the restoration of mechanical properties.

2. Materials and methodology

2.1 Materials

To study the effect of the different additives, four mortar mixtures were designed, being a reference mixture without additives, a mixture with SAPs, a mixture with nanosilica and a mixture containing both SAP and nanosilica. The cement used is Portland cement CEM I 52.5N Strong from Holcim. River sand 0/2 was added as small aggregate in an amount of 2 to 1 with respect to the weight of the binder. The water-to-binder ratio was kept constant at 0.35. Due to the relatively low amount of mixing water, a superplasticizer was added in an amount of 0.4% compared to the binder weight to increase the workability. The superplasticizer used was MasterGlenium 51 (concentration 35%) from BASF. Note that, as nanosilica acts as a binder, cement was replaced partially by nanosilica in the concerned mixtures to maintain the binder quantity.

The type of superabsorbent polymer used is a copolymer of acrylamide and sodium acrylate. The SAP is produced by bulk polymerization and provided by BASF. The particle size is equal to 100 ± 21.5 µm in the dry state and can swell up to a size of 257 ± 55 µm in demineralized water [33]. Whereas generally larger sizes of SAPs are utilized to promote self-healing, this SAP was chosen owing to the limited reduction of the compression strength noticed in previous research [13]. Moreover, the self-healing capacity of cementitious mixtures including the SAP under study demonstrated its beneficial effect [3] [13]. The amount of SAPs added was set at 0.2% by weight of the binder. Additional water was added to the mortar mixtures with SAPs to account for their water uptake. By means of a flow table test, following NBN EN 1015-3 [34], an identical workability of the reference and SAP mixture was obtained for an additional amount of 26 grams of water per gram of SAP. The SAPs were added to the mixing bowl in the dry state and the additional water was added together with the mixing water and dissolved superplasticizer.

The nanosilica used within this study is a colloidal silica, namely LUDOX® HS40, and was obtained from W. R. Grace & Co.-Conn (Antwerp, Belgium). The dispersion contains 40% of synthetic amorphous silica by mass. The nominal diameter of the nanosilica particles is approximately equal to 12 nm and the specific surface area lies between 198 and 258 m^2/g. The amount of nanosilica amounts to 2% of the total weight of the binder and was chosen as it counteracted the strength loss due to SAP inclusion, investigated in previous research [13]. In this way, the mortar with SAPs and nanosilica has an identical compressive strength with respect to the reference material, which would be important for future load-bearing purposes. Note that this amount refers to the dry silica particles and not to the suspension. Mortar mixtures with nanosilica contained an increased amount of superplasticizer equal to 0.76%, as the inclusion of nanosilica drastically lowered the workability. Superplasticizer was added instead of water, as the nanosilica was unable to retain the water long enough to ensure an equal amount of mixing water during the hydration stage. To improve the dispersion of the nanosilica particles, the colloidal solution was placed in an ultrasonic bath for five minutes, prior to its addition to the cementitious blend.

2.2 Sample preparation

For every mixture composition, three mortar prisms measuring 30 mm x 30 mm x 360 mm were cast with a central steel reinforcement bar of 6 mm diameter and a length of 700 mm, depicted in Figure 1 (a). It can be seen that a central line was drawn, used for the positioning of the sensors during the healing assessment. The specimens were cured in plastic foil for 28 days at 20 ± 2°C. The cracking of the specimens was then executed by means of a tensile

test, using an Instron 5982 Floor Model Testing System with a capacity of 100 kN, as can be seen in Figure 1 (b). The steel reinforcement was clamped within the testing device and a tensile load was exerted at a speed of 0.01 mm/s. Due to the elongation of the steel bar, the mortar showed multiple cracking. On average six cracks were formed. The test was continued until no new cracks appeared and an average crack width between 100 µm and 200 µm was maintained after unloading.

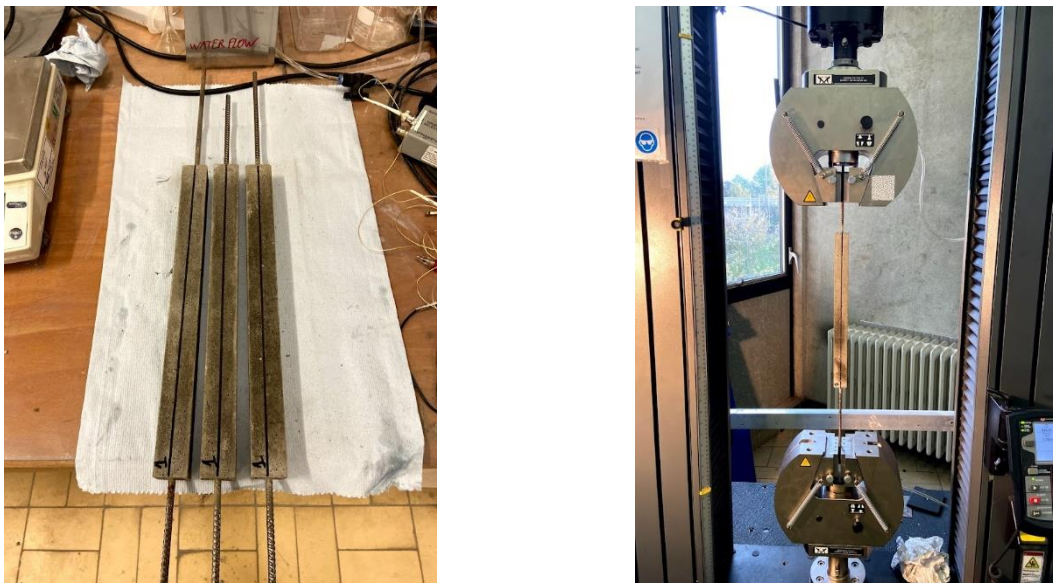

(a) (b)

Figure 1: Photographs of (a) the mortar specimens and (b) the tensile test set-up.

After cracking, the specimens were placed in wet-dry curing cycles for 28 days to promote the crack healing mechanism. The cycles consisted of 1 hour submersion in water at 20 ± 2°C and 23 hours of dry conditions at 20 ± 2°C and 65 ± 5% RH.

2.3 Ultrasonic surface wave measurements

The monitoring of the crack closure was performed by ultrasonic surface wave measurements. The set-up consisted in the placement of two sensors on the surface of the specimen, at the position of the center line, using a thin layer of vacuum grease as a coupling agent. The specific sensors (“pico” type) are relatively broadband sensors, operating between 50 and 800 kHz. Their peak sensitivity lies at 450 kHz and their size is equal to 5 mm. The distance between the sensors was 30 mm (center to center) in all experiments. The excitation of a wave signal was conducted by means of mechanical pencil lead breaks. This is a standardized source, often used in literature, to produce broadband excitations for ultrasonic measurements [35]. Every measurement was repeated five times, alternating the position of the pencil; i.e. closer to the left or right sensor. A schematical representation of the test method can be seen in Figure 2.

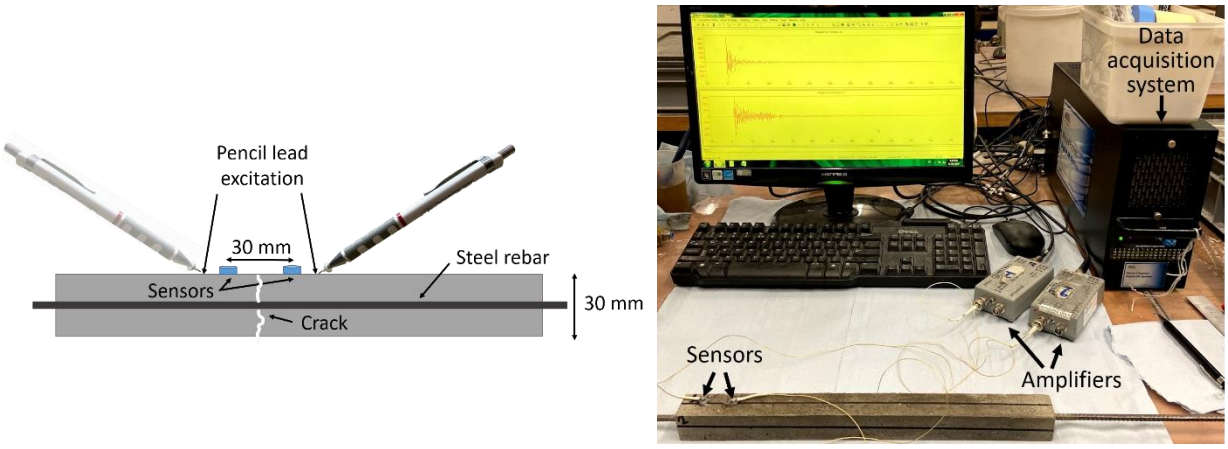

Figure 2: Schematical representation of the ultrasonic surface wave measurements, showing the placement of the sensors and the pencil lead break test (left) and laboratory set-up (right).

The assessment of the self-healing evolution was performed by an analysis of different wave parameters, namely the longitudinal wave velocity and the attenuation. In Figure 3, two waveforms received from a pencil lead break test on an intact mortar specimen are shown. The terms '1st sensor' and '2nd sensor' signify the closest and furthest sensor w.r.t. the pencil lead break, respectively. The first crossing of the threshold, defined as the maximum noise level of the received waveform during the "pre-trigger" stage, signifies the arrival of the longitudinal wave, which is by definition the fastest mode. Knowing the distance between the sensors, the longitudinal wave velocity can be calculated as the distance divided by the travel time between the sensors. For the example in Figure 3, a travel time 6.6 µs was found, leading to a velocity of 4545 m/s. Later, the arrival of the Rayleigh cycle can be distinguished by a more severe deviation of the amplitude from the noise level.

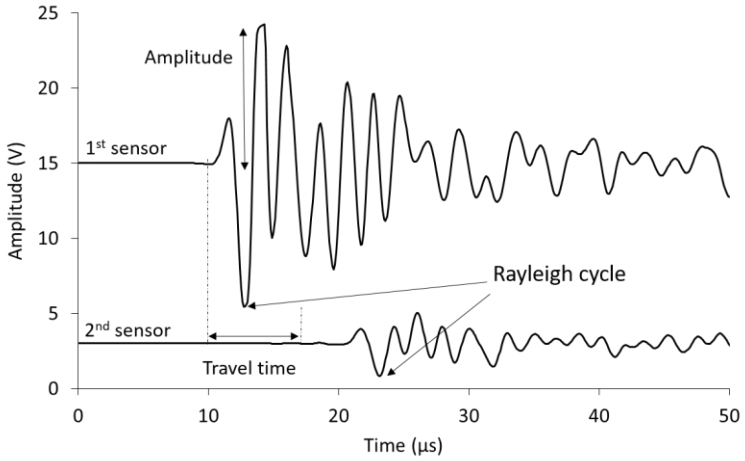

Figure 3: Typical waveforms received from a pencil lead break test on an uncracked mortar specimen.

Apart from the wave velocity, attenuation provides important information on the propagation path. Attenuation is defined as the reduction in wave amplitude as the signal propagates a certain distance (between the two sensors). Scattering on aggregates and voids, cracks and damping within the matrix material contribute to the total amplitude loss. Looking at the example waveforms in Figure 3, the amplitude of the first sensor is equal to 9.24 V, whereas the amplitude at the second sensor is 2.05 V. The attenuation is calculated using Equation 1:

$$Attenuation\ \left[\frac{dB}{mm}\right] = -\frac{1}{D} * 20 * log\left(\frac{A_2}{A_1}\right) \quad [1]$$

where A_1 and A_2 are the amplitudes in Volts of the closest and furthest sensor, respectively. D is the distance between the sensors (30 mm in this case). An attenuation value of 0.44 dB/mm was obtained for the example case.

To monitor the self-healing evolution, this procedure was repeated at various moments within the wet-dry curing cycles. At first, the uncracked state was evaluated after 28 days of curing in plastic foil. The specimens were then cracked and from each specimen, one to two separated cracks were chosen to be followed-up by ultrasound. This was done in order to eliminate any interaction of nearby cracks on the ultrasonic measurements, which could provide immediate reflection of the emitted wave signal. The measurements took place immediately after cracking and after 3, 7, 14 and 28 days of curing in wet-dry cycles. The steel reinforcement bars were wrapped with parafilm to avoid possible corrosion. To eliminate the influence of the specimen's degree of saturation on the ultrasound results, the tests were each time performed at the same moment within the curing cycles, being 16 hours after the submersion in water.

2.4 Numerical simulations

Numerical simulations were performed using the commercially available software Wave2000 Plus [36]. The software utilizes a method of finite difference to solve the 2D elastic wave equations. The specific acoustic equation that is simulated is:

$$\rho \frac{\partial^2 u}{\partial^2 t} = \left(\mu + \eta \frac{\partial}{\partial t}\right) \nabla^2 u + \left(\lambda + \mu + \varphi \frac{\partial}{\partial t} + \frac{\eta}{3} \frac{\partial}{\partial t}\right) \nabla(\nabla \cdot u) \quad [3]$$

where u is the displacement vector (yielding two components u_x and u_y that are perpendicular to each other), t [s] is the time, ρ [kg/m³] is the density, λ [Pa] is the first Lamé constant, μ [Pa] is the second Lamé constant, η [Pa·s] is the shear viscosity and φ [Pa·s] is the bulk viscosity.

The simulated geometry is a two-dimensional representation of the experimental series and can be seen in Figure 4. The length of the specimen was limited to 70 mm instead of the 360 mm of the mortar samples, while infinite boundary conditions were implemented at the edges to omit any reflections from these surfaces. The source had a size of 1 mm, resembling the pencil lead used during the experiments, and was placed at 10 mm from the closest sensor. A single sine cycle was emitted with a frequency of 450 kHz, being the peak frequency of the experimental sensors. A set of sensors with a size of 5 mm, equal to the size of the pico sensors, was placed on the surface, separated by a distance of 30 mm. The spatial resolution of the geometry was equal to 0.05 mm and the simulation time was set at 100 μs.

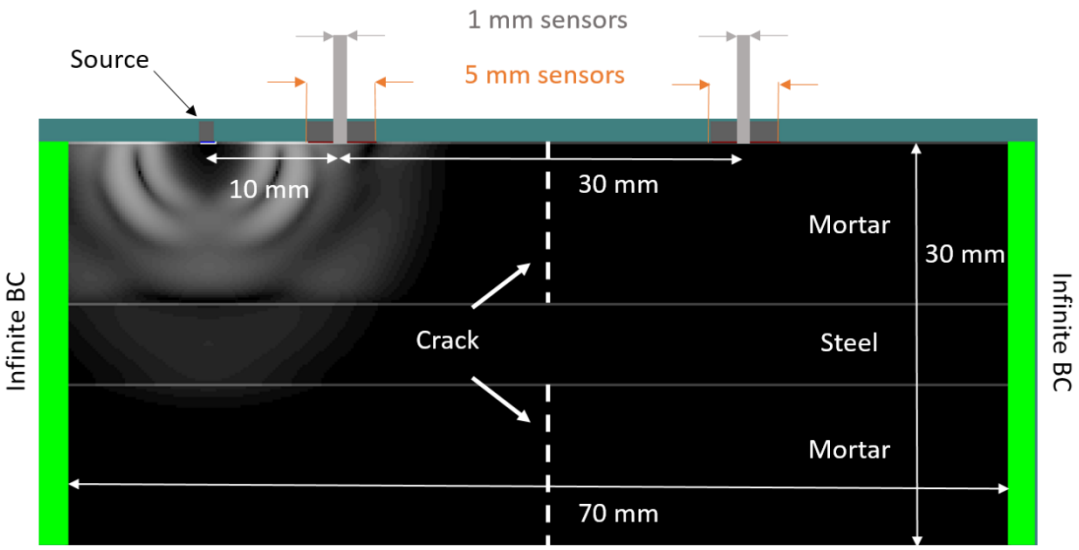

Figure 4: Geometry of the simulation model, indicating the position of the source and sensors.

Concerning the material properties allocated to the model, the characteristics of the reference mortar were used. The bulk density of the mortar was equal to 2170 kg/m³. From typical ultrasonic measurements performed on the identical mortar mixtures without steel reinforcement, an E-modulus of 27 GPa and a Poisson's ratio of 0.3 were found. For the steel reinforcement, a density of 7850 kg/m³, stiffness of 210 GPa and Poisson's ratio of 0.3 were inserted. Concerning damping coefficients for the mortar, these were adapted until an attenuation value of 0.32 dB/mm, matching the experimental results (Appendix Table 1, attenuation for uncracked material) was reached. In case of the steel reinforcement, for which attenuation is expected negligible, the coefficients were chosen by the software's material database, resulting in an attenuation value of 0.03 dB/mm. Lastly, the crack was simulated by an air gap in the upper and lower layers of mortar, keeping the intact steel reinforcement in place (see dashed lines in Figure 4. The air gap was centred with respect to the sensors and had a width of 200 µm. The properties of air were a density of 1.2 kg/m³ and a longitudinal wave velocity of 330 m/s.

3. Results and discussion

3.1 Experimental series

A global view on the evolution of the received waveforms throughout the experiments is studied. Figure 5 depicts the evolution of the waveforms of a representative reference specimen throughout the entire testing procedure. After cracking (2nd sensor cracked in Figure 5Figure 3), it was noticed that the waveform received by the sensor positioned after the discontinuity with respect to the excitation signal (see Figure 2) showed a strong decrease in amplitude compared to the uncracked situation. The created discontinuity within the travel path practically prohibited the wave to pass to the second sensor. Additionally, the Rayleigh cycle can no longer be identified, due to the loss of shear rigidity upon cracking. The specimen was then placed in wet-dry cycling, in order to promote the self-healing mechanism. Looking at the evolution of the waveforms, a gradual restoration of the amplitude values, as well as of the travel time can be observed between 3 and 28 days of healing. This partial amplitude restoration and transit time decrease suggest that partial crack closure occurred.

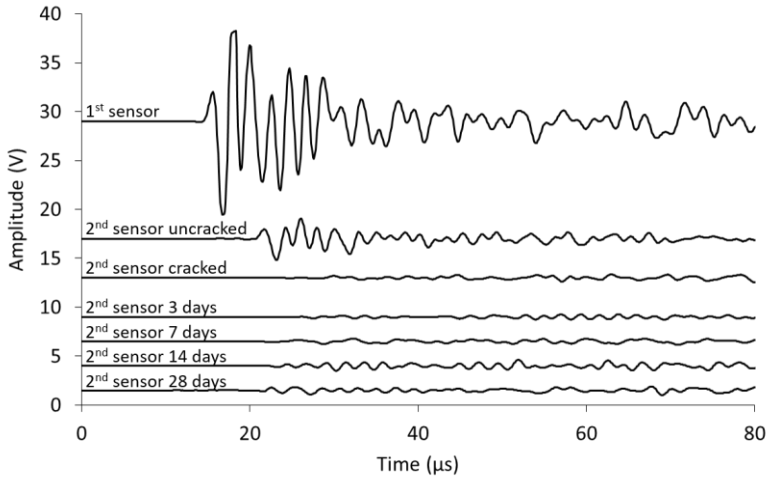

Figure 5: Evolution of the waveforms during wet-dry curing of a representative reference specimen. The waveforms are shifted upwards for clarity.

An analysis of the longitudinal wave velocity and attenuation was performed. The values shown in Figure 6 represent the average of all ultrasonic measurements conducted for each mixture series, being five pencil lead breaks per crack, for a total of three to six monitored cracks. The standard deviations are not included in the graphical representations below, in order to increase the comprehensibility of the observed trends. However, Appendix Table 1 summarizes the experimental results and their coefficient of variation. In Figure 6 (a), the changes in the longitudinal wave velocity are presented with respect to the time. At day 0, two measurements per mixture composition were performed, being one in the uncracked state and one in cracked conditions. Velocities in between 4300 and 4700 m/s were obtained before cracking, indicating a good quality of the mixtures [37]. However, the mortar blends with SAPs show lower velocities compared to the reference material, due to the increased macroscopic porosity. As expected, the crack creation lowered the velocity drastically, as the discontinuity prohibited the signal to follow the shortest path between both sensors. The wave could only reach the second sensor through locally present contact points between the crack walls, caused by crushed debris during unloading, or through refraction from the tip of the crack at the position of the reinforcement bar, something that noticeably increases the travel distance. During healing, the longitudinal wave velocity increased again, leading to a partial restoration of the original velocity value. From Figure 6 (a), a more pronounced improvement during the first week was detected for reference, SAP and HS40 mixtures, while the combination of SAPs and nanosilica demonstrated a more continuous increase over the entire healing period. This phenomenon will be clarified later upon discussion of the exact numbers. Nevertheless, the increment in wave velocity suggested partial healing for all tested mixtures.

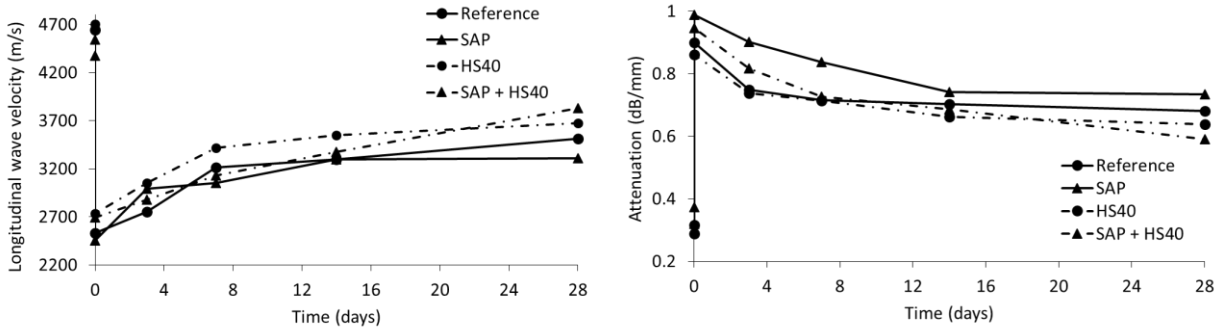

(a) (b)

Figure 6: Evolution of (a) longitudinal wave velocity and (b) attenuation vs. time.

Figure 6 (b) depicts the development of the attenuation over time. Initially, the attenuation was relatively low, though higher for the SAP mortar compared to the other mixtures. The introduction of the crack posed a discontinuity within the matrix, which strongly increased the attenuation, from approximately 0.3 dB/mm to almost 1 dB/mm. Again, the application of wet-dry curing cycles partially restored the attenuation values, yielding a significant reduction in attenuation within the first three to seven days of healing and a more gradual decrease afterwards. The mortar with SAPs and HS40 showed a more continuous decrease in attenuation with respect to the other mixtures.

To allow for a more thorough comparison between the different mixtures, the restoration in terms of velocity and attenuation were calculated and are presented in Figure 7. This property was defined as the difference between the healed and the cracked parameter values, compared to the degradation of this parameter upon cracking, and was calculated using Equation 2:

$$Restoration\ [\%] = \frac{Q_{av.,healed} - Q_{av.,cracked}}{Q_{av.,uncracked} - Q_{av..,cracked}} * 100 \quad [2]$$

where $Q_{av.,X}$ signifies the average of the parameter under study, namely the wave velocity or attenuation, at stage X (uncracked, cracked or healed). The exact values, together with the standard deviation between the three specimens, are summarized in Appendix Table 1. The restoration of the longitudinal wave velocity, detailed in Figure 7 (a), showed an increase for all studied mixtures. However, some discrepancies between the mixture compositions can be observed. In case of the reference, a restoration of about 10% was obtained during the first three days of wet-dry curing. A continuation of these cycles then showed a further improvement to 33% after seven days of healing, which indicates that further hydration and precipitation of $CaCO_3$ occurred, thanks to the regular water supply through wet-dry curing. Yet, after 14 days of wet-dry cycles, the improvement slowed down, most likely due to a shortage of unhydrated cement and $Ca(OH)_2$. A similar evolution was observed for the restoration of the attenuation (Figure 7 (b)), which increased strongly during the first week of healing and stagnated afterwards. On the other hand, the SAP mortar demonstrated a significant improvement in terms of velocity within the first three days of curing, which can be attributed to the prolonged water supply. Afterwards, the recovery slowed down and a slightly higher restoration percentage compared to the reference was obtained. The inclusion of nanosilica contributes to autogenous healing by its pozzolanic reaction with $Ca(OH)_2$. During the first three days of wet-dry curing, a recovery of the longitudinal velocity equal to 21% was noticed, showing an improvement compared to the reference, but less effective than the addition of SAPs. Between three and seven days of healing, the restoration percentage increased more strongly, i.e. from 21% to 43%. Most likely, the continued hydration that occurred upon the placement in wet-dry curing cycles led to the formation of $Ca(OH)_2$ inside the crack, which then reacted with nanosilica to form CSH. Lastly, the combination of SAPs and HS40 revealed a slow development of the healing process during the first three healing days. Afterwards, the recovery accelerated and a considerable restoration percentage of 57% was obtained after 28 days of wet-dry curing in terms of wave velocity and 63% in terms of attenuation. These results confirm the inherent self-healing ability of cementitious mixtures without additives and acknowledge the benefit of SAPs and nanosilica for the promotion of self-healing.

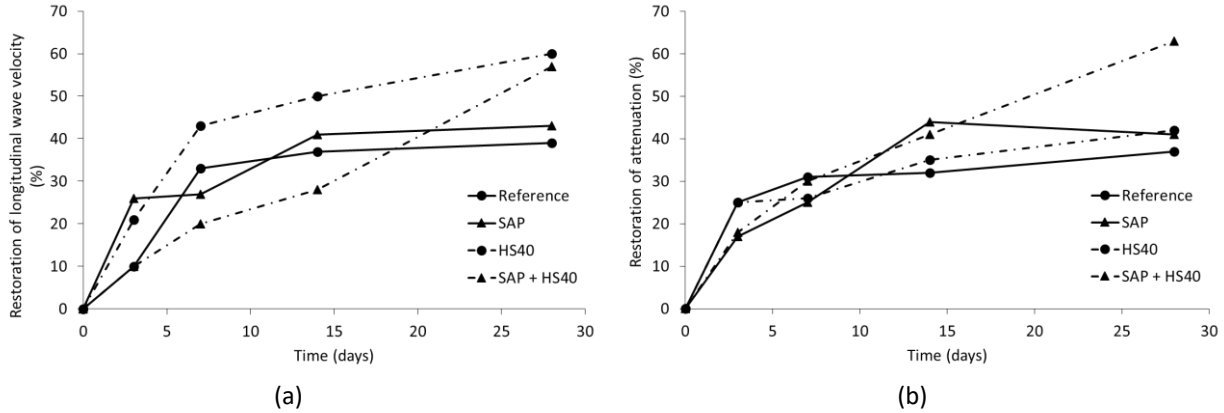

(a) (b)

Figure 7: Restoration of (a) longitudinal wave velocity and (b) attenuation after healing vs. time.

The restoration of the wave parameters during wet-dry curing implies a certain change in the wave's travel path, as well as the existence of physical compounds inside the crack. Still, these parameters do not allow for a quantification of the actual filling of the crack, neither of the stiffness of the self-healing compounds. To get an insight in these features, numerical simulations are of paramount importance.

3.2 Numerical simulations

Figure 8 depicts the simulated waveforms captured by the sensors in the uncracked and cracked state. The upper waveform represents the signal received by the closest sensor. The arrival at the 2nd sensor corresponds to a wave velocity of 4615 m/s, similar to the experiments. The amplitude in the second sensor has decreased compared to the one in the first sensor, also seen during the experiments, leading to an attenuation of 0.32 dB/mm. Next, the air gap was created in between the two sensors with a thickness of 200 µm, going through the mortar solely, to simulate the crack. Similar to the conducted measurements, the arrival time was delayed resulting in a decrease of the longitudinal wave velocity by about 800 m/s, leading to a value of 3845 m/s after cracking. In addition, the attenuation was largely increased compared to the uncracked situation, increasing from 0.32 dB/mm to 0.65 dB/mm.

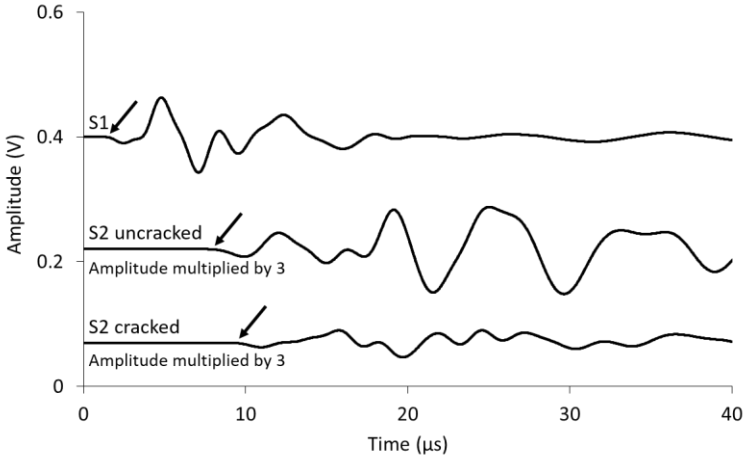

Figure 8: Waveforms received from the numerical simulations. The waveforms are shifted upwards for clarity. The arrows indicate the arrival of the longitudinal wave.

After the crack creation, the effect of filling the crack space was studied. For the numerical simulations, two indicative cases of healing were considered, specifically a partially healed and a completely healed crack, depicted in Figure 9. In case of a partially healed crack, a healing layer was placed within the top and bottom 3 mm of the crack, while in deeper layers, closer to the reinforcement bar, the air gap was maintained. This specific healing case was considered as it was reported in literature that autogenous healing mostly takes place close to the surface [38] [32]. The completely healed situation concerns the filling of the entire crack with healing material.

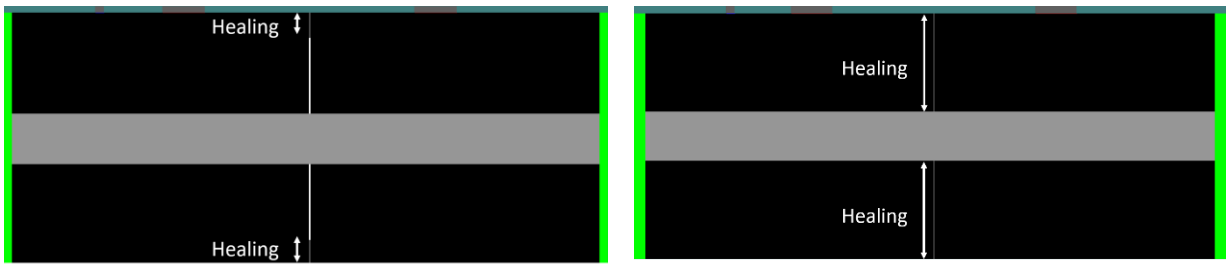

(a) Partially healed (b) Completely healed

Figure 9: Representation of (a) partially healed and (b) completely healed simulation cases.

In order to model the process of self-healing, the basic properties of the healing material were varied, namely elastic modulus and density. Regarding the E-modulus, 5 different cases were simulated, being 0.01 GPa, 0.1 GPa, 1 GPa, 10 GPa and 70 GPa. This selection spans all possible orders of magnitude of stiffness from nearly negligible to the ideal stiffness of pure $CaCO_3$ crystals, which are abundantly formed throughout the autogenous healing process [38], even though practically this value is not expected to be achieved within the narrow crack. Besides, it was decided to use two density values, namely 2711 kg/m³ (equal to the density of pure $CaCO_3$ in accordance to above) and 1600 kg/m³, which is notably lower than the ideal situation to account for the likely possibility that the healing will result in compounds that deviate from the ideal condition. Nevertheless, it will be seen that the density only had a marginal effect on the results.

First, the results of the completely healed situation are discussed. Figure 10 (a) depicts the longitudinal wave velocity obtained. It was observed that the variation of the healing products' stiffness strongly affected the wave velocity. Additionally, within the range of low stiffness values, the velocity increased steeply, whereas between 1 GPa and 10 GPa, and later between 10 GPa and 70 GPa, the slope was reduced. These results indicate that the filling of the crack, even with a low-stiffness material, influences the propagation of ultrasonic waves significantly. Also, the original velocity before cracking, i.e. about 4615 m/s, should be reached between 10 GPa and 70 GPa. These trends were visible for both densities used. The effect of variable density on the simulated wave velocity was below 1%, making no practical difference. The attenuation values obtained from the fully healed simulation model are presented in Figure 10 (b). The attenuation varied between 0.65 dB/mm in the cracked state and 0.29 dB/mm in case of pure $CaCO_3$ filling, showing the decreasing trend of attenuation with stiffness. The reduction was more pronounced up to 1 GPa, while the decrease slowed down afterwards. Also, the attenuation obtained for a stiffness of 10 GPa and 70 GPa was lower than the attenuation of 0.32 dB/mm seen for the uncracked situation, meaning that a complete recovery was obtained.

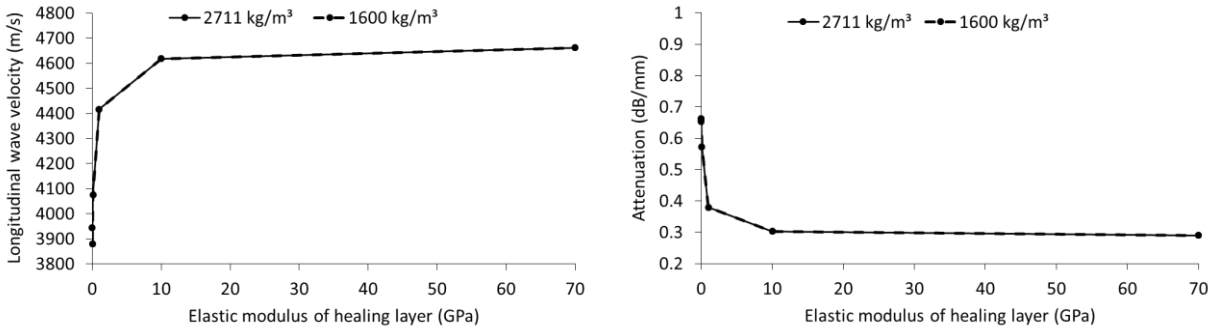

(a) (b)

Figure 10: (a) Longitudinal velocity and (b) attenuation vs. elastic modulus of the healing layer in case of complete healing for densities of 1600 kg/m³ and 2711 kg/m³.

Next, the simulation results with a partially healed crack are presented. As the density showed to only have a marginal influence on the outcome, the different densities will not be discussed in-depth. Figure 11 shows the partially and completely healed stages, having a healing layer density of 1600 kg/m³. The longitudinal velocity (see Figure 11 (a)) showed a similar development compared to the completely healed case, being approximately 3% lower for the partial healing. Concerning the attenuation, the results in Figure 11 (b) were closely related to the completely healed situation. A slightly increased attenuation was seen up to a stiffness of 1 GPa, after which nearly identical values were reached. These results indicate that, in terms of attenuation, partial healing is sufficient to restore the wave propagation as measured with this main frequency (450 kHz) and this sensor size (5 mm).

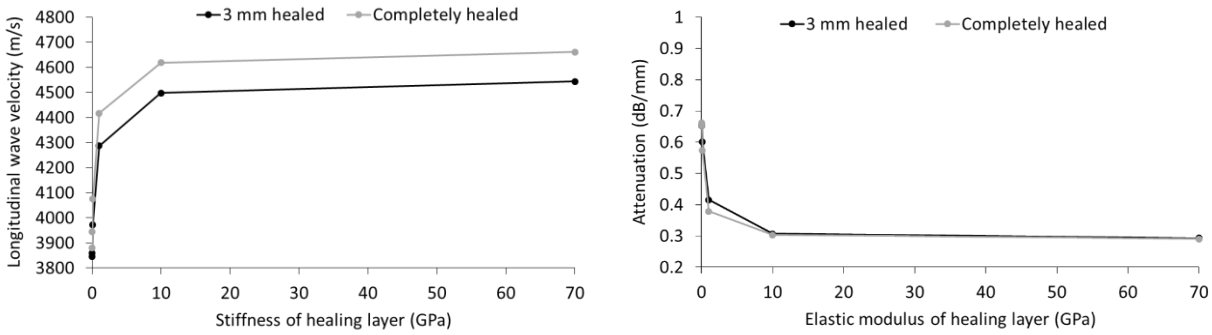

(a) (b)

Figure 11: (a) Longitudinal velocity and (b) attenuation vs. elastic modulus of the healing layer in case of a partially and completely healed crack.

The snapshots of the transient displacement fields in Figure 12 (a) and (b) reveal the wave propagation path at different timings during the numerical simulations in the cracked and partially healed stages, respectively. In the cracked situation (a), the wave was mostly reflected onto the boundary of the created air gap, whereas only a small part of the signal was able to pass to the second sensor through the crack tip on top of the steel reinforcement. The surface or Rayleigh wave was completely reflected onto the crack opening. Concerning the partially healed situation, the simulations demonstrated the transmission of both the longitudinal and the Rayleigh wave through the healing layer inserted at the top of the crack, which led to a shortened travel path and thus an increased wave velocity and amplitude.

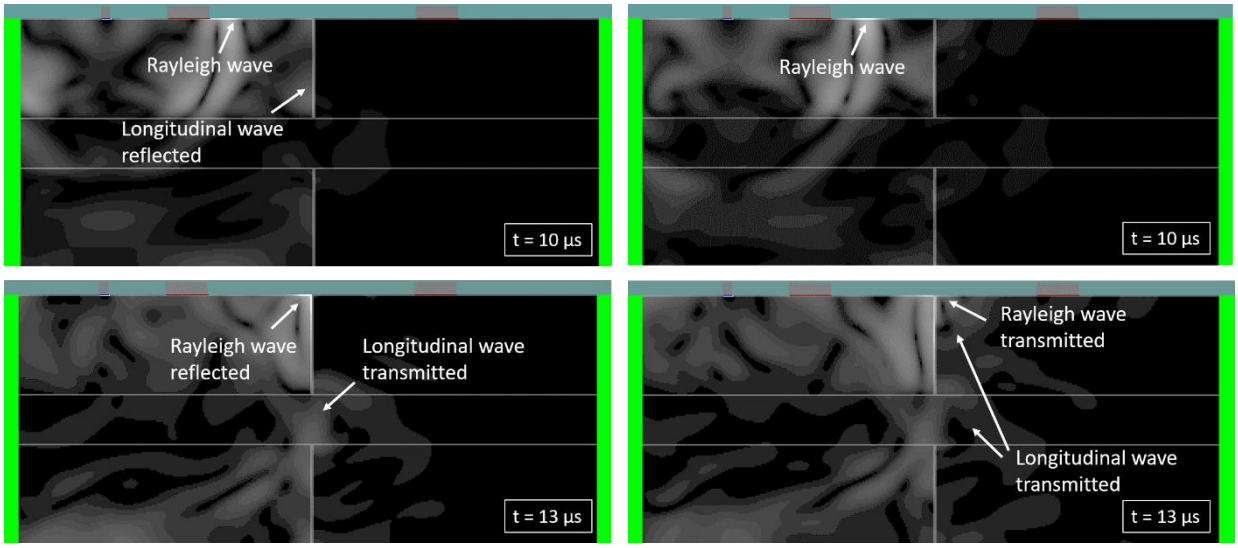

Figure 12: Snapshots of the wave simulations in (a) cracked stage and (b) partially healed situation with an elastic modulus of 10 GPa. The green boundaries signify infinite boundary conditions.

The numerical results demonstrate the excellent sensitivity of ultrasound to the stiffness of the healing layer, especially at the crucial initial phase where the stiffness develops from practically zero to 1 GPa. Within this region of developing stiffness values, the velocity showed an increase up to 550 m/s, which equals 12% of the uncracked velocity. Still, even for later increases in stiffness from 1 GPa to 10 GPa, the longitudinal wave velocity increased by approximately 200 m/s. A similar, even more pronounced, trend can be seen for the attenuation, as the relative decrease between 1 GPa and 10 GPa amounts to 19% and is mostly attributed to the reduced reflection between the mortar and the stiffening healing compounds.

Finally, the restoration percentages obtained from the numerical simulations are summarized in Figure 13. A table summarizing the exact values for a density of 1600 kg/m³ can be found in the Appendix. Regarding the restoration of the longitudinal wave velocity, a similar, increasing trend was observed for both healing cases with increased stiffness of the healing layer. However, an improved recovery was seen for a completely filled crack, due to the increased transmission of the signal. Similarly, the restoration of the attenuation demonstrated an increasing value for higher stiffness of the healing layer, i.e. up to 109%. When comparing the outcome of a 3 mm healing layer to a completely healed crack, the restoration was noticeably different for low stiffness values only (up to 1 GPa). At higher stiffness, the restoration percentage was approximately identical, meaning that stiff healing compounds close to the surface can restore the attenuation as measured for this frequency and sensor size. The Rayleigh wavelength, calculated by the Rayleigh velocity (approximately 2500 m/s) divided by the basic signal frequency of 450 kHz, is equal to 5.5 mm. Therefore, for the specific experimental case, most of the energy would anyway propagate through a shallow layer, also seen in [39]. The distinction between partial and complete healing is thus not expected to be straightforward. However, lower frequencies, yielding deeper penetration, could be used to characterize the filling percentage.

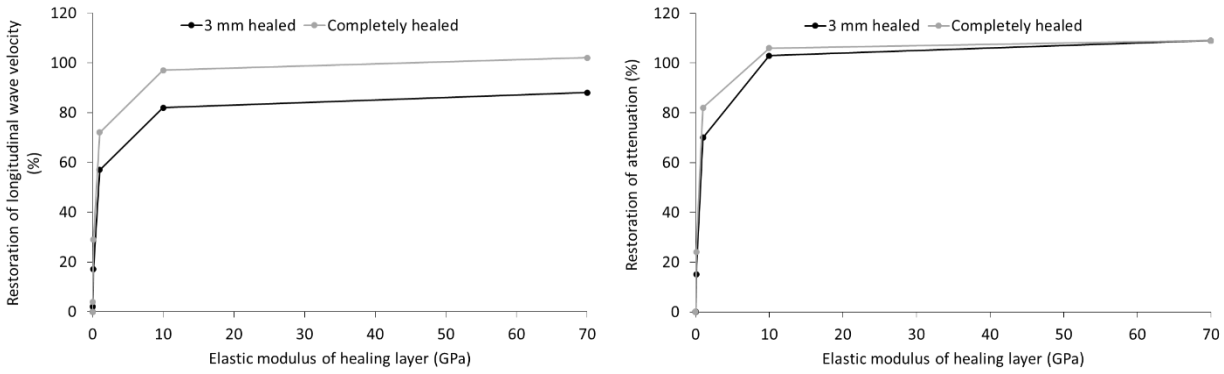

Figure 13: Restoration of (a) longitudinal wave velocity and (b) attenuation vs. elastic modulus of the healing layer for partially and completely healed simulation stages.

During the experimental series, a recovery of the longitudinal wave velocity up to 43% was noticed in case of a mortar including SAPs and even 60% for the addition of nanosilica, indicating a considerable crack filling effect. Considering the restoration based on the simulations, as shown in Figure 13, a restoration percentage of 43% matched the range of healing stiffness between 0.1 GPa and 1 GPa, in case of both partial and complete healing, whereas 60% restoration is situated between 0.1 GPa and 1 GPa for partial healing and between 1 GPa and 10 GPa for complete healing. These results thus suggest a relatively low stiffness of the formed healing layer, which seems likely if one considers the healing circumstances of the experimental series. Foremost, the mechanism of autogenous healing depends on multiple factors, such as the availability of unhydrated cement, $Ca(OH)_2$ and moisture. When these components are absent or consumed, autogenous healing no longer takes places. Secondly, the mortar specimens were cracked by means of a tensile test, leading to multiple, through-going cracks. The only connection between the crack walls was the steel reinforcement bar, which was situated in the centre. The number of precipitation surfaces was therefore limited, while literature demonstrated the benefit of having a high amount of precipitation surfaces, which can be accomplished by the addition of fibres [40]. These reasons imply that the order of stiffness of the healing products is certainly lower than the mortar itself, something in agreement with the restoration of wave parameters. The ultrasonic surface wave measurements thus showed to be valuable to assess the closure of the cracks, while the combination with the numerical simulations allowed for a non-destructive estimation of the stiffness of the healing layer for the first time in literature.

3. Conclusion

Within this study, the self-healing effectiveness of cementitious mortars was assessed by means of surface ultrasonic wave measurements. To promote autogenous healing, superabsorbent polymers and nanosilica were added to the mixtures and wet-dry curing was applied. Through an analysis of the longitudinal wave velocity and the attenuation, the evolution of the crack healing was evaluated, demonstrating a partial restoration of these parameters for all mixtures, after the initial significant change due to cracking. Whereas comparable trends were noticed for each mixture composition, the blends with SAPs and/or nanosilica showed an improved recovery of the wave parameters.

Besides the conducted experiments, numerical simulations were performed to validate the sensitivity of ultrasound to a developing healing layer. Whereas the density of the healing layer only marginally influenced the obtained wave parameters, a significant recovery of the longitudinal wave velocity and attenuation was observed for elastic moduli within the range of 0.01 GPa and 1 GPa, while still being measurable for higher stiffnesses between 1 GPa and 70 GPa. This validates the sensitivity of US to the stiffness development within the healing layer and its characterization potential for self-healing composites. Besides, a comparison between a partially and completely filled crack

demonstrated a noticeably higher velocity in case of complete filling, while the attenuation showed to differ for low stiffness values (below 10 GPa) only. The latter was ascribed to the specific conditions of the measurements, utilizing a frequency of 450 kHz, which limits the possibility to differentiate between partial and complete healing. For this reason, different excitation frequencies could supply a solution, since they define the penetration depth of the Rayleigh waves. In addition, ultrasonic mapping using transmission measurements would prove useful, disclosing the improvements within the entire crack cross-section.

The combination of experiments and simulations points to a measurable recovery due to self-healing, while exposing the relatively low stiffness of the healing products, i.e. mostly between 0.1 GPa and 1 GPa, based on the relative restoration. It should be highlighted that the importance of this study lies in the disclosure of the sensitivity of different wave parameters to the existence of a crack and healing, rather than to exactly match the experimental and numerical values during the whole process. Discrepancies were noticed in terms of exact values and can be explained by the differences between the simulated geometry and the actual specimens. In the numerical simulations, a 2D representation of the set-up is used and the attenuation was fitted to the experimental one, to account for damping as well as spreading of the beam. However, it is supposed that 3D simulations could be more appropriate to accommodate the actual 3D spreading of the wave beam. Additionally, the discussion of wave velocity focused on the longitudinal wave, since the Rayleigh cycle was not identified after cracking. The first observable disturbance is always attributed to longitudinal waves, either directly transmitted (uncracked case) or through contact points (cracked and healed cases). However, attenuation can be considered as a measure of the total transmission. In the intact state, the peak amplitude at both sensors can be safely attributed to Rayleigh waves, as seen for example in Figure 3. However, for latter cases, and especially the first measurement after cracking, Rayleigh waves were not identified as already discussed. Therefore, even though the attenuation is not attributed to the Rayleigh cycle, it is still a parameter that monotonically changes with healing and can be used for the evaluation of the process. Another point related to ultrasound is that the size of the sensors is known to influence the amplitude through the “aperture effect” [41] [42]. This effect is stronger for surface waves and was inevitably included in the experimental measurements. Therefore, although numerical simulations with smaller, point sensors are possible, simulations from 5 mm sensors were presented to exercise the same aperture effect with the experiment. The present study confirms the potential of ultrasonic monitoring for self-healing purposes. The combination with numerical simulations allowed to estimate the stiffness of the formed healing products and paves the way for ultrasound to be used for self-healing evaluation.

4. Acknowledgements

The authors wish to express their gratitude to Dr. Alexander Assmann (BASF) for providing the SAP under study and to Yves De Vreese (W. R. Grace & Co.-Conn.) for providing LUDOX® HS40.

[1] K. Van Tittelboom and N. De Belie, “Self-Healing in Cementitious Materials - A Review,” *Materials,* vol. 6, pp. 2182-2217, 2013.

[2] H. Huang, G. Ye, C. Qian and E. Schlangen, “Self-healing in cementitious materials: Materials, methods and service conditions,” *Materials and Design,* vol. 92, pp. 499-511, 2016.

[3] D. Snoeck and N. De Belie, “Autogenous healing in strain-hardening cementitious materials with and without superabsorbent polymers: an 8-year study,” *Frontiers in Materials,* vol. 6:48, pp. 1-12, 2019.

[4] D. Snoeck, J. Dewanckele, V. Cnudde and N. De Belie, “X-ray computed microtomography to study autogenous healing of cementitious material promoted by superabsorbent polymers,” *Cement and Concrete Composites,* vol. 65, pp. 83-93, 2016.

[5] P. Chindasiriphan, H. Yokota and P. Pimpakan, “Effect of fly ash and superabsorbent polymer on concrete self-healing ability,” *Construction and Building Materials,* vol. 233, p. 116975, 2020.

[6] C. Schröfl, K. Erk, W. Siriwatwechakul, M. Wyrzykowski and D. Snoeck, “Recent progress in superabsorbent polymers for concrete,” *Cement and Concrete Research,* vol. 151, p. 106648, 2022.

[7] F. Sanchez and K. Sobolev, “Nanotechnology in concrete - A review,” *Construction and Building Materials,* vol. 24, pp. 2060-2071, 2010.

[8] A. Said, M. Zeidan, M. Bassuoni and Y. Tian, “Properties of concrete incorporating nano-silica,” *Construction and Building Materials,* vol. 36, pp. 838-844, November 2012.

[9] H. Du, S. Du and X. Liu, “Durability performances of concrete with nano-silica,” *Construction and Building Materials,* vol. 73, pp. 705-712, December 2014.

[10] O. Öztürk, G. Yildirim, U. Keskin, H. Siad and M. Sahmaran, “Nano-tailored multi-functional cementitious composites,” *Composites Part B: Engineering,* vol. 182, p. 107670, 2020.

[11] A. Pourjavadi, S. Fakoorpoor, P. Hosseini and A. Khaloo, “Interactions between superabsorbent polymers and cement-based composites incorporating colloidal silica nanoparticles,” *Cement and Concrete Composites,* vol. 37, pp. 196-204, 2013.

[12] G. Olivier, R. Combrinck, M. Kayondo and W. Boshoff, “Combined effect of nano-silica, super absorbent polymers, and synthetic fibres on plastic shrinkage in concrete,” *Construction and Building Materials,* vol. 192, pp. 85-98, 2018.

[13] G. Lefever, D. Snoeck, D. Aggelis, N. De Belie, S. Van Vlierberghe and D. Van Hemelrijck, “Evaluation of the self-healing ability of mortar mixtures containing superabsorbent polymers and nanosilica,” *Materials,* vol. 13, no. 2, p. 380, 2020.

[14] A. Suleiman, A. Nelson and M. Nehdi, “Visualization and quantification of crack self-healing in cement-based materials incorporating different minerals,” *Cement and Concrete Composites,* vol. 103, pp. 49-58, 2019.

[15] J. Wang, J. Dewanckele, V. Cnudde, S. Van Vlierberghe, W. Verstraete and N. De Belie, “X-ray computed tomography proof of baterial-based self-healing in concrete,” *Cement and Concrete Composites,* vol. 53, pp. 289-304, 2014.

[16] E. Gruyaert, B. Debbaut, D. Snoeck, P. Diaz, A. Arizo, E. Tziviloglou, E. Schlangen and N. De Belie, “Self-healing mortar with pH-sensitive superabsorbent polymers: testing of the sealing efficiency by water flow tests,” *Smart Materials and Structures,* vol. 25, no. 8, p. 084007, 2016.

[17] T. Van Mullem, E. Gruyaert, B. Debbaut, R. Caspeele and N. De Belie, “Novel active crack width control technique to reduce the variation on water permeability results for self-healing concrete,” *Construction and Building Materials,* vol. 203, pp. 541-551, 2019.

[18] S. Qian, J. Zhou, M. de Rooij, E. Schlangen, G. Ye and K. van Breugel, “Self-healing behavior of strain hardening cementitious composites incorporating local waste materials,” *Cement and Concrete Composites,* vol. 31, no. 9, pp. 613-621, 2009.

[19] H.-W. Reinhardt, C. Grosse and A. Herb, “Ultrasonic monitoring of setting and hardening of cement mortar - A new device,” *Materials and Structures,* vol. 33, pp. 580-583, 2000.

[20] X. Wang and K. Subramaniam, “Ultrasonic monitoring of capillary porosity and elastic properties in hydrating cement paste,” *Cement and Concrete Composites,* vol. 33, no. 3, pp. 389-401, 2011.

[21] S. Popovics, “Analysis of the Concrete Strength versus Ultrasonic Pulse Velocity Relationship,” *Materials Evaluation,* vol. 59, no. 2, pp. 123-130, 2001.

[22] V. Haach, L. Marrara Juliani and M. Ravanini Da Roz, “Ultrasonic evaluation of mechanical properties of concretes produced with high early strength cement,” *Construction and Building Materials,* vol. 96, pp. 1-10, 2015.

[23] F. Silva, J. Delgado, R. Cavalcanti, A. Azevedo, A. Guimaraes and A. Lima, “Use of nondestructive testing of ultrasound and artificial neural networks to estimate compressive strength of concrete.,” *Buildings,* vol. 11, no. 2, p. 44, 2021.

[24] J.-F. Chaix, V. Garnier and G. Corneloup, “Ultrasonic wave propagation in heterogeneous solid media: Theoretical analysis and experimental validation,” *Ultrasonics,* vol. 44, no. 2, pp. 200-210, 2006.

[25] P. Antonaci, C. Bruno, A. Gliozzi and M. Scalerandi, “Monitoring evolution of compressive damage in concrete with linear and nonlinear ultrasonic methods,” *Cement and Concrete Research,* vol. 40, no. 7, pp. 1106-1113, 2010.

[26] E. Ahn, M. Shin, J. Popovics and R. Weaver, “Effectiveness of diffuse ultrasound for evaluation of micro-cracking damage in concrete.,” *Cement and Concrete Research,* vol. 124, p. 105862, 2019.

[27] E. Ahn, H. Kim, S. Sim, S. Shin and M. Shin, “Principles and applications of ultrasonic-based nondestructive methods for self-healing in cementitious materials,” *Materials,* vol. 10, no. 3, p. 278, 2017.

[28] M. Ait Ouarabi, P. Antonaci, F. Boubenider, A. Gliozzi and M. Scalerandi, “Ultrasonic monitoring of the interaction between cement matrix and alkaline silicate solution in self-healing systems,” *Materials,* vol. 10, no. 1, p. 46, 2017.

[29] L. Camara, M. Wons, I. Esteves and R. Medeiros-Junior, “Monitoring the self-healing of concrete from the ultrasonic pulse velocity,” *Journal of Composites Science,* vol. 3, no. 1, p. 16, 2019.

[30] N. Kaur, S. Majhi, N. Dhami and A. Mukherjee, “Healing fine cracks in concrete with bacterial cement for an advanced non-destructive monitoring,” *Construction and Building Materials,* vol. 242, p. 118151, 2020.

[31] G. Lefever, D. Snoeck, N. De Belie, S. Van Vlierberghe, D. Van Hemelrijck and D. Aggelis, “The contribution of elastic wave NDT to the characterization of modern cementitious media,” *Sensors,* vol. 20, no. 10, p. 2959, 2020.

[32] S. Fan and S. Li, “X-ray computed microtomography of three-dimensional microcracks and self-healing in engineered cementitious composites,” *Smart materials and structures,* vol. 24, no. 1, p. 015021, 2014.

[33] D. Snoeck, O. Jensen and N. De Belie, “The influence of superabsorbent polymers on the autogenous shrinkage properties of cement pastes with supplementary cementitious materials,” *Cement and Concrete Research,* vol. 74, pp. 59-67, August 2015.

[34] Belgisch instituut voor normalisatie (BIN), *Methods of test for mortar masonry - Part 3: Determination of consistence of fresh mortar (by flow table),* 1999.

[35] RILEM Technical Committee (Masayasu Ohtsu), “Recommendation of RILEM TC 212-ACD: Acoustic emission and related NDE techniques for crack detection and damage evaluation in concrete: Measurement method for acoustic emission signals in concrete.,” *Materials and Structures,* vol. 43, no. 9, pp. 1177-1181, 2010.

[36] Cyberlogic, “Wave2000 Plus - Software for Computational Ultrasonics,” Available online: http://www.cyberlogic.org/wave2000.html, accessed on January 28 2022.

[37] T. Naik, V. Malhotra and J. Popovics, “The ultrasonic pulse velocity method,” in *Handbook on Nondestructive Testing of Concrete, Second Edition*, 2003, p. Chapter 8.

[38] D. Snoeck and N. De Belie, “Repeated autogenous healing in strain-hardening cementitious composites by using superabsorbent polymers,” *Journal of Materials in Civil Engineering,* vol. 28, no. 1, p. 04015086, 2015.

[39] D. Aggelis, T. Shiotani and D. Polyzos, "Characterization of surface crack depth and repair evaluation using Rayleigh waves," *Cement and Concrete Composites,* vol. 31, no. 1, pp. 77-83, 2009.

[40] Y. Yang, E.-H. Yang and V. Li, “Autogenous healing of engineered cementitious composites at early age,” *Cement and Concrete Research,* vol. 41, pp. 176-183, 2011.

[41] N. Ospitia, D. Aggelis and G. Lefever, “Sensor size effect on Rayleigh wave velocity on cementitious surfaces,” *Sensors,* vol. 21, no. 19, p. 6483, 2021.

[42] E. Tsangouri and D. Aggelis, “The influence of sensor size on acoustic emission waveforms - a numerical study,” *Applied Sciences,* vol. 8, no. 2, p. 168, 2018.

Appendix Table 1: Longitudinal wave velocity (m/s), restoration of longitudinal wave velocity after healing (%), attenuation (dB/mm) and restoration of attenuation after healing (%) of the mortar mixtures in the cracked, uncracked and healed stages, together with the coefficient of variation (n = 3).

		Longitudinal wave velocity (m/s)	Restoration of longitudinal wave velocity after healing (%)	Attenuation (dB/mm)	Restoration of attenuation after healing (%)
Reference	Uncracked	4647 ± 7%	n/a	0.32 ± 31%	n/a
	Cracked	2534 ± 12%	n/a	0.90 ± 20%	n/a
	3 days	2753 ± 17%	10 ± 130%	0.75 ± 16%	25 ± 8%
	7 days	3215 ± 11%	33 ± 24%	0.72 ± 29%	31 ± 10%
	14 days	3269 ± 15%	37 ± 54%	0.70 ± 20%	32 ± 60%
	28 days	3378 ± 3%	39 ± 8 %	0.68 ± 13%	37 ± 24%
SAP	Uncracked	4376 ± 6%	n/a	0.37 ± 38%	n/a
	Cracked	2452 ± 10%	n/a	0.99 ± 12%	n/a
	3 days	2994 ± 13%	26 ± 35%	0.90 ± 17%	17 ± 71%
	7 days	3051 ± 9%	27 ± 67%	0.84 ± 17%	25 ± 16%
	14 days	3297 ± 10%	41 ± 29%	0.74 ± 14%	44 ± 30%
	28 days	3311 ± 6%	43 ± 2%	0.73 ± 10%	41 ± 15%
HS40	Uncracked	4703 ± 12%	n/a	0.29 ± 41%	n/a
	Cracked	2733 ± 10%	n/a	0.86 ± 29%	n/a
	3 days	3051 ± 14%	21 ± 110%	0.74 ± 23%	25 ± 92%
	7 days	3419 ± 7%	43 ± 67%	0.71 ± 27%	26 ± 12%
	14 days	3548 ± 7%	50 ± 48%	0.66 ± 17%	35 ± 37%
	28 days	3677 ± 7%	60 ± 55%	0.62 ± 27%	42 ± 57%
SAP + HS40	Uncracked	4542 ± 8%	n/a	0.32 ± 38%	n/a
	Cracked	2694 ± 7%	n/a	0.95 ± 19%	n/a
	3 days	2878 ± 7%	10 ± 50%	0.82 ± 17%	18 ± 72%
	7 days	3128 ± 9%	20 ± 35%	0.73 ± 34%	30 ± 43%
	14 days	3374 ± 11%	28 ± 39%	0.69 ± 16%	41 ± 10%
	28 days	3832 ± 4%	57 ± 14%	0.59 ± 19%	63 ± 22%

Appendix Table 2: Longitudinal wave velocity (m/s), restoration of longitudinal wave velocity after healing (%), attenuation (dB/mm) and restoration of attenuation after healing (%) of the numerical simulations for partial and complete healing and varying stiffness of the healing layer.

		Longitudinal wave velocity (m/s)	Restoration of longitudinal wave velocity after healing (%)	Attenuation (dB/mm)	Restoration of attenuation after healing (%)
	Uncracked	4645	n/a	0.32	n/a
	Cracked	3845	n/a	0.65	n/a
3 mm healed	0.01 GPa	3860	2	0.65	0
	0.1 GPa	3977	17	0.60	15
	1 GPa	4302	57	0.42	70
	10 GPa	4502	82	0.31	103
	70 GPa	4549	88	0.29	109
Fully healed	0.01 GPa	3879	4	0.66	-3
	0.1 GPa	4075	29	0.57	24
	1 GPa	4417	72	0.38	82
	10 GPa	4618	97	0.30	106
	70 GPa	4662	102	0.29	109